光電子分光を用いた物性研究 : 装置から研究の基礎さらに強相関電子系研究のフロンティアまで(第51回 物性若手夏の学校(2006年度))

AUTHOR(S):

菅, 滋正

CITATION:

菅, 滋正. 光電子分光を用いた物性研究 : 装置から研究の基礎さらに強相関電子系研究のフロンティアまで(第51回 物性若手夏の学校(2006年度)). 物性研究 2007, 87(5): 756-790

ISSUE DATE:

2007-02-20

URL:

http://hdl.handle.net/2433/110766

光電子分光を用いた物性研究：
装置から研究の基礎さらに強相関電子系研究のフロンティアまで

大阪大学大学院基礎工学研究科　菅　滋正
suga@mp.es.osaka-u.ac.jp

はじめに

光電子分光（Photoelectron spectroscopy：PES と略す）はいまや固体の電子物性研究のもっとも有力な手段の一つである。前世紀初頭 Einstein によって提案された光量子説においてもこの光電効果が重要な役割を果たした。放電管や X 線管の利用で実用になった光電子分光は、1970 年代からは放射光光源の利用によって新しい局面を迎えた。角度分解光電子分光、共鳴光電子分光、定始状態分光、定終状態分光、飛行時間差分光、偏光依存性測定等の手法の開発が続いた。アンジュレーター光源の利用もこの発展を強力に推進した。放射光分光光学系も電子エネルギー分析器も進化を遂げた。特に静電半球型電子エネルギー分析器の高性能化に伴い、2 次元検出器を用いた角度分解光電子分光の発展は著しい。

今世紀に入ると軟 X 線・硬 X 線領域での高分解能測定や、10eV 程度以下で超高分解能の光電子分光が実用になるなど、この分野は現在さらに一段の大飛躍の局面に入った。

光電子は運動エネルギーによって変わる非弾性平均自由行程（λ_{mp}）を持つことが知られているが、これが極小では３－５A 程度となるために極めて表面に敏感な計測法と考えられる。従って表面研究には極めて適した手法である。たとえば後に述べる電子相関が弱い半導体の場合でも表面再構成や表面緩和が起こった場合に表面の電子状態は大きく変わることが予想される。この場合には表面敏感な光電子スペクトルは内部電子状態のスペクトルとは大きく異なることになる。また表面再構成や表面緩和が起こらない場合でも、最近接原子数がバルクの場合の約半分となるので、電子の移動エネルギーt はバルクの値の約半分となる。一方電子相関エネルギー(2 電子間の Coulomb 反発エネルギー)U は表面でもバルクでもそれほど変わらない。そうすると U/t はバルクに比べて表面では約 2 倍になる。強相関電子系の電子状態は U/t が大きい場合には絶縁体的になり、これが小さいときは遍歴性が増し金属的になる傾向が知られている。それゆえバルク電子状態を探るには表面敏感性の大きな運動エネルギーE_K が 20－100eV 程度の測定ではなく、バルク敏感性の高い数百 eV あるいは数千 eV、あるいは物質によっては５　eV 程度以下の光電子分光が必要となる。

3 日間にわたる本講義では、筆者の 30 年間に渡る研究をベースにして、各国の放射光源を含む種々の光源、分光光学系、分光手法、解析法、物性研究例、トピックス、周辺関連手法、諸外国の状況、今後の展望などを講義することを考えている。

Contents

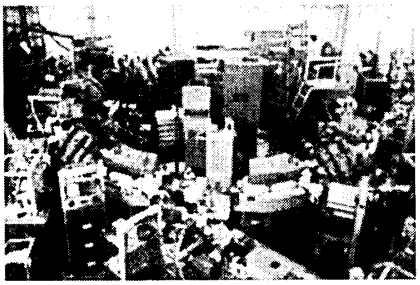

世界最初の放射光専用電子蓄積
リング　SOR-RING(物性研)

1.Introduction

Photoelectric effects were first observed by Hertz in 1887 through the spark between two electrodes by illumination of the negative electrode by ultraviolet light. Thompson discovered the electron in 1897 and Lenard demonstrated in 1900 that this effect is associated with the emission of electrons from the metal under ultraviolet light. From the dependence of the emitted electron current on the light intensity and the electron velocity on the light frequency, Einstein proposed in 1905 the concept of photons. The concept of the work function is also recognized around this time. The validity of the Einstein's theory of the photoelectric effect was established around 1916 by Millikan. Many metals were also carefully studied and the Einstein's equation was confirmed (1928 Lukirsky).

The question whether the photoelectric effect is a pure surface effect or a bulk effect was raised and unsettled for a long time since the vacuum of the experimental systems was rather poor. Considerable efforts were also made to determine the work functions of many materials. It was found in 1923 that the work function of W was significantly lowered by Cs coverage (Kingdon and Langmuir).

From the application point of view, the lowering of the work function by means of Cs deposition was applied in the form of Ag-O-Cs cathode to detect infrared. Similar technique is now often used for negative electron affinity cathode to have a sensitivity down to $h\nu$=0.9 eV or to prepare the spin polarized electrons from GaAs by circularly polarized laser light. The photoelectric effect is now used for photomultiplier in wide $h\nu$ region.

By late 1950's the understanding of electronic structures of simple solids was noticeably advanced. A photoelectron spectroscopy (PES) is reported in Si (Spicer and Simon 1962), where the PES is compared with the optical spectra and band structures. Then a lot of experimental works were done on tetrahedral semiconductors. Development of theoretical works followed in accord. The concept of k-conserving direct transition and nonconserving transition is intensively discussed (Spicer) in early 1960's.

The early PES was performed below $h\nu$~6eV. The PES in higher $h\nu$ was performed in the vacuum ultraviolet with use of hydrogen lamps separated from the experimental chamber by LiF windows with a cut off at $h\nu$~11.8eV in mid 1960's. The use of synchrotron radiation for PES became a reality in late 1960's at DESY. The use of storage ring instead of electron synchrotron became a major stream after mid 1970's qwing to the beam stability in storage rings. Even in the case of VUV lamp sources, the extension of the $h\nu$ toward higher energies became feasible by He discharge lamps with the removal of the LiF windows. The UHV condition is realized in the experimental

chamber by differential pumping because the capillary is installed in front of the He lamp. This lamp can provide a strong discrete line at hν=21.2eV (HeI) (Turner, 1962) and a weaker line at hν=40.8eV (HeII) under low pressures. Due to the narrow line width of the strong HeI line source, even the molecular vibration levels are studied in the case of gaseous samples (1970, Turner et al.).

Siegbahn and collaborators started to realize a high resolution photoelectron spectrometer for X-ray photoelectron spectroscopy (XPS) in 1951. It was soon found that sharp peaks were observed corresponding to core levels. The origin of XPS can be traced back to early 1910's. However, the energy resolution around that time was very bad. When X-ray absorption and emission spectroscopy became popular, XPS was almost abandoned. Four decades later, the sharp peaks observed in XPS, which were much sharper than absorption and emission spectra, opened new applications such as the electron spectroscopy for chemical analysis (ESCA). The Kα lines of Al and Mg are nowadays most often used for conventional XPS. However, the width of these characteristic lines is ~1eV. By use of bent quartz crystals, the resolution down to 0.2eV was achieved for the Al Kα line at the sacrifice of the intensity (1974 Siegbahn). XPS in the valence band region is thought to provide information on density of states modified by the photoionization cross sections of constituent electronic states.

Now conventional PES systems are often equipped with both He lamp and X-ray tube to study both valence band and core levels. The UHV conditions are satisfied and the surface cleaning instruments are installed. However, there is a gap between the hν of the He lamp and the X-ray tube. The middle energy region is covered by synchrotron radiation (abbreviated as SR) source. Although the hν resolution was much improved for HeI and for laser light sources below 7eV now, the efforts to realize high resolution by SR are still under way. For high resolution PES at hν beyond HeI source, the use of SR combined with high resolution monochromator is inevitable.

From mid 1970's the angle resolved photoelectron spectroscopy (ARPES) became feasible utilizing the energy and momentum conservation to study the band dispersion, where the momentum parallel to the specular surface is thought to be conserved during the electron escape from the surface. The momentum perpendicular to the surface is thought not to be conserved. For low dimensional (2D or 1D) materials with negligible dispersion to the perpendicular direction, the ARPES at one hν can provide enough information on band dispersion. For three dimensional materials, the band dispersion depends also upon the momentum perpendicular to the surface. In this case, the tunable hν source as SR is inevitable combined with normal emission ARPES measurements. Off-normal ARPES measurement is performed by means of 1) rotating a

small analyzer with angular resolution or 2) rotating the sample in front of the analyzer. 3) use of a two dimensional detector behind the exit slit of the hemispherical analyzer. In addition, 4) really two dimensional detectors are now developed which can detect the full angular distribution simultaneously.

The use of synchrotron radiation enabled the resonance photoemission with tuning hν in a particular core excitation region, enhancing a particular electronic state as a result of interference between direct photoemission and the direct recombination following the core excitation. Such states as f and d outer shell states buried in strong valence band structures can be effectively probed.

In accord with the development of spin detectors, angle integrated and resolved PES measurements with spin resolution became feasible for ferromagnetic materials. The spin polarization is also observed for nonmagnetic materials excited by circularly polarized light as a result of the spin orbit interaction.

Although abundant information is obtained on occupied electronic states by PES, less was known for unoccupied states. The inverse photoemission spectroscopy (IPES) became available for the study of unoccupied states in early 1980's. The angle resolved IPES can provide information on the band dispersion of the unoccupied states. When the spin polarized electrons are used, the spin resolved and angle resolved IPES is also feasible.

PES, ARPES and IPES are all relatively surface sensitive methods. There are more surface sensitive techniques like scanning tunneling spectroscopy. On the other hand more bulk sensitive spectroscopies are also required. Such related means are also briefly lectured.

2. Background

In PES studies the concept of the inelastic mean free path of photoelectrons is quite important. The electron-electron interaction induces the finite and rather short inelastic mean free path, which is in the range of 3-5A between 20 and 100eV of kinetic energies E_K. Therefore the PES in this energy region is generally surface sensitive. Although this quantity depends upon the individual material, it is widely accepted that it increases below 10eV and above 100eV. Therefore a special caution is required to study bulk electronic structures by PES. In the case of strongly correlated electron systems, the surface electronic structures are noticeably different from the bulk electronic structures. In order to overcome this difficulty, high resolution PES below 10eV and above a few hundred eV is now strongly desired. The latter is promoted in many synchrotron facilities by developing brighter undulator light sources, high

transmittance and high resolution monochromators, and high performance electron analyzers. As for low energy high resolution PES, the resolution better than 1meV is already achieved and development of light sources as well as high performance monochromators are under way. Many examples of the high energy and low energy bulk sensitive high resolution PES are explained in the lecture. As for the electron analyzer, the performance of the spherical analyzer is amazingly improved in the last few years and can realize the resolution better than 1meV in the low energies and ~50meV in a few keV region.

ARPES provides important information on the momentum dependence of the electron energies. As well known the momentum resolution is in proportion to the square root of the electron kinetic energy. Therefore the ARPES is feasible even in the soft X-ray region in a few hundred eV without difficulty. However, the inelastic mean free path is still in the order of 10 to 15A and some contribution from the surface is not fully negligible. Although much higher bulk sensitivity is achieved in a few keV, ARPES becomes more difficult due to the worsened momentum resolution and low count rates. In the case of extremely low energy ARPES below the kinetic energy of 5 eV (ELEPES), the matrix element effect is very strong and the measurement in a wide region of the Brillouin zone is not a simple task.

In order to realize an extreme bulk sensitivity for the study of momentum dependence of electronic structures, resonant inelastic X-ray scattering (RIXS) analysis can be employed. In this case the probing depth can be easily >10μm and one can cover few Brillouin zones by properly rotating both the sample and the Rowland circle. One of the advantage of RIXS is that even the insulator could be studied without the problem of charging up. Therefore RIXS is a powerful complementary tool to study the metal-insulator transition systems.

In accord with the development of nanotechnology, PES of micro and nano-materials are under strong interest. By focusing the high brilliance SR and scanning the sample, scanning photoelectron microscope (SPEM) with the lateral resolution better than 100 nm becomes feasible. If only the secondary electrons are detected, photoelectron emission microscopy (PEEM) is applicable to nano materials with the lateral resolution down to 20 nm. In the case of magnetic materials, magnetic circular and/or linear dichroism is utilized to realize the contrast of the magnetic domains. In the case of quantum well states (QWS) in thin films, the confinement is perpendicular to the surface and the dispersion parallel to the surface can be observed by ARPES. Further the time resolution is now utilized for PES experiments. The aspects of high resolutions in energy, momentum, space and time are useful key issues

in materials sciences.

3.Instrumentation

1) Synchrotron radiation, undulator radiation and other light sources

The photoelectrons can be excited by photons which have enough energy higher than the so-called work function (ϕ) of materials. In most cases of solids, ϕ is around 5 eV. Therefore photons with the energy $h\nu$ larger than 6eV are usually required for the measurement of photoelectrons to cover the region of ~1eV from the Fermi level (E_F) in the conventional case of one photon excitation. This is not the case for two photon excitation. The wavelength λ (A) is related to $h\nu$ (eV) by the equation of $\lambda(A)=12398.4/h\nu(eV)$.

Traditionally X-ray tubes and He light sources have been used for the conventional photoelectron spectroscopy. The $h\nu$ are 1253.6 eV for the Mg Kα, 1486.6 eV for the Al Kα, 21.2eV for the HeI and 40.8eV for the HeII light sources. The full width at half maximum (FWHM) of the X-ray tube is ~1eV which could be improved down to 0.4 or 0.3eV by use of crystal monochromators. The FWHM of the HeI sources is conventionally of the order of 0.1eV. Newly developed RF excited He source, however, achieves the FWHM of the order of 1meV. Other sources can be also used for the excitation.

The characteristics of the synchrotron radiation emitted by relativistic electron with the velocity of the electron very close to the light velocity c in circular storage rings are summarized as 1) wide $h\nu$ spectral distribution from infrared to γ-rays facilitating tunability of monochromatized photons in a wide $h\nu$ region. 2) linearly polarized in the orbital plane and elliptically polarized slightly above or below this plane. 3) instantaneously emitted to the tangential direction of the orbit. 4) divergence of the radiation is $1/\gamma$ (where the Lorentz factor γ is equal to ~1957E, when the energy of the electrons accelerated in the storage ring is E(GeV)). Therefore the divergence is of the order of 6.4×10^{-5} radian in the case of 8 GeV storage ring. 5) not a cw light source but a pulsed light source with a quite accurate repetition. The pulse-to-pulse time delay is 2 ns, for example, for 500MHz RF (radio frequency) acceleration if all the bunches are filled up. The FWHM of each pulse can be in the range of 0.1 to few ns depending upon the individual storage ring design and operation mode. It is possible to fill only a single bunch or few bunches on the orbit. Then the pulse-to-pulse delay can be even 5 μs when only one bunch is filled around the circumference of 1.5 km, since the velocity of the electron is very close to the light velocity which is 3×10^8 m/s. 6) very long 1/e decay time

of the order a few hours to a hundred hour, providing very stable photon flux.

The fundamental parameters of the storage rings are the curvature (radius) of the bending magnet ρ(m), magnetic field intensity H (kG), electron energy E (GeV). The electron rest mass energy m_0c^2 is 0.51 MeV and $\gamma=E/m_0c^2$. The Lorentz force provides the relation of $\rho=10^{10}E/cH$. The critical wavelength λ_c (A) of the bending radiation is given by

$$\lambda_c=4\pi\rho/3\gamma^3=186/HE^2.$$

Although the decrease of the photon flux on the lower hν side is gradual, the decrease on the higher hν side is rapid and one order of magnitude decreases at $0.1\lambda_c$. When the higher hν is required for the bending radiation, higher energy storage ring with higher H in the bending magnet is required.

The higher energy storage ring, however, requires both higher H and higher RF power, because the energy loss of the electron per revolution is proportional to E^4/ρ. The cost effective way to generate higher hν photons by lower energy storage ring is to insert a high magnetic field device in the straight section of the storage ring. Although the E is kept as it is, higher H provides a smaller λ_c. If such a high H device has periodic magnetic structures with the up and down field directions alternatively and the period number is N, the photon flux can be N times increased. In this case the electron follows the wiggling orbit. Such a device is called a wiggler and often employed in low energy storage rings to deliver higher hν photons. In these cases, the radiation is not coherent. The maximum deviation angle ϕ_0 of the electron orbit in the wiggler from the central orbit can be expressed by $K\gamma^{-1}$ where $K=0.0934H_0\lambda_u$(H_0(kG) is the magnetic field of the wiggler and λ_u(m) is the length of the single period of the wiggler). When K is much larger than 1, ϕ_0 is larger than the natural divergence of $1/\gamma$. Then the spectral distribution of the wiggler is just as the bending radiation.

The radiation from the bending magnets is finally emitted into 360° horizontal angle, whereas the vertical divergence is still $1/\gamma$. It is usually necessary to collect the radiation in a wide horizontal angle to get high photon flux. In the case of wiggler radiation, total horizontal spread depends upon ϕ_0 which can be K times larger than $1/\gamma$.

If K is smaller than 1, ϕ_0 becomes smaller than $1/\gamma$. Then the emitted light intensity from one particular electron passing through this device is always non zero in the forward direction. Then rather monochromatic radiation is available on the optical axis. Since the magnetic field required for this device is very low, short period of the magnetic lattice is feasible and the period number N up to 1000 is not impossible. This device is called an undulator, where the light emitted from the preceding period can interfere with the radiation from the succeeding period resulting in the partial coherence. Thus

the undulator radiation from this device is at least N times stronger and the interference further induces the narrowing of the energy spread of the fundamental and higher order harmonic radiations. Thus undulator radiation has very high brilliance represented by photon numbers/s/mrad^2/mm^2/1%band width. There are two types of undulators: one is a planar undulator with the alternative up and down magnetic fields and the other is a helical undulator with the helical field. By defining the K values for the x (horizontal) and y (vertical) directions as K_x and K_y, the direction of the radiation from the undulator axis as θ, the wavelength of the n–th harmonics is represented as

$$\lambda_n=\lambda_u(1+(K_x^2+K_y^2)/2+\gamma^2\theta^2)/2n\gamma^2.$$

The undulator period length ranges usually from few mm to a few tens cm. It is therefore possible to change the energy of the undulator radiation by changing the K value(s). In the case of permanent magnet undulators, the tuning is often done by varying the gap distance of the dipole magnet. In contrast to the case of the wigglers, the increase of the magnetic field results in the decrease of hν. It is also seen that the off axis radiation has always lower hν. In the case of helical undulator, the radiation on the axis is mostly composed of the fundamental radiation (n=1) because the velocity of the electrons to the observer on the axis is always constant. In the case of planar undulators the relative velocity of the electrons to the observers changes with time and higher order harmonics are stronger than the case of helical undulator particularly in the off axis direction. The quantitative theoretical derivation of the synchrotron radiation is given by considering the Lienard-Wiechert retardation potential.

Now free electron lasers (FEL) are under development in several facilities to provide coherent pulsed laser light with fs FWHM. The energy resolution is in this case limited by the uncertainty principle expressed in the form of $\Delta t\cdot \Delta E \geq h/2\pi$ (0.65meV for 1ps).

The polarization properties of SR will be discussed later.

2) Priniciple of grating and crystal monochromators

Since conventional SR has a wide energy spread, monochromators are required to obtain monochromatic radiation. Even in the case of undulators monochromators are required to perform high resolution experiment. The reflection grating monochromators are often used in the hν range from few eV up to 2000 eV and crystal monochromators are often used above 1500 eV.

The principle of diffraction by the grating is given by the following diffraction equation where α is the incidence angle and β is the exit angle measured from the macroscopic surface normal of the grating. In many cases blazed gratings are employed

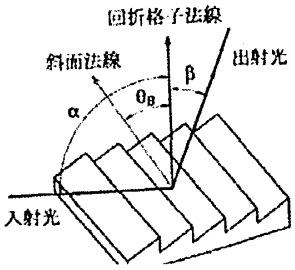

ブレーズ回折格子の模式図

for monochromatizing vacuum ultraviolet and soft X-rays. The definition of the blaze angle θ_B as well as α and β is given in the above figure. If the period or the lattice constant is d, the optical path difference between the two beams incident on the neighboring facet is expressed as $d(\sin\alpha-\sin\beta)$ with the positive sign for both α and β in the case shown in this figure. When this quantity is equal to $m\lambda$ (m is an integer and λ is the photon wave length), the interference between the two beams takes place and a monochromatic light is diffracted to the β direction. m can be either positive or negative and the diffraction under such conditions are called positive order light or negative order light. The light reflected for $\alpha=\beta$ satisfies m=0 and is called 0^{th} order light which contains wide $h\nu$ components and is not usually used for spectroscopy.

In the case of diffraction gratings the m-th order light with the wave length of λ/m is also diffracted to the β direction and overlaps with the 1^{st} order light with the wave length of λ. It is very important to suppress the higher order lights to have a high quality spectroscopy data. For this purpose, the total reflection by mirrors is often employed to suppress higher order lights. This technique is called order sorting. In the soft X-ray region with the wave length λ, the refractive index $n(\lambda)$ of many materials (Au, Pt, and so on) coated on gratings is usually smaller than 1.0. For the incidence angle of α onto the mirror, the total reflection takes place for α larger than $\alpha_c=\sin^{-1}n$. At this incidence angle, the photons with lower $h\nu$ (or longer λ) is totally reflected and the higher $h\nu$ photons are suppressed. Spherical grating monochromators have been traditionally employed in the soft X-ray region. If the curvature (radius) of the spherical grating is R, a circle with a diameter R (therefore radius is R/2) called Rowland circle is often considered. When the Rowland circle is in contact with the spherical grating at its center, and the entrance slit and exit slit are located on this Rowland circle, a horizontal focusing condition is satisfied according to the focusing equation of

$$\cos^2\alpha/r - \cos\alpha/R+\cos^2\beta/r'-\cos\beta/R=0,$$

where the α and β are the incidence and exit angle as defined before. r and r' are the distance of the entrance and exit slits from the center of the grating. Most of high resolution grating monochromators have been based on the Rowland mount so far.

However, nowadays varied line spacing plane gratings became available by means of the original ruling by diamond cutter or by ion beam etching. Without using the concept of Rowland circle, the focusing is realized by the grating itself.

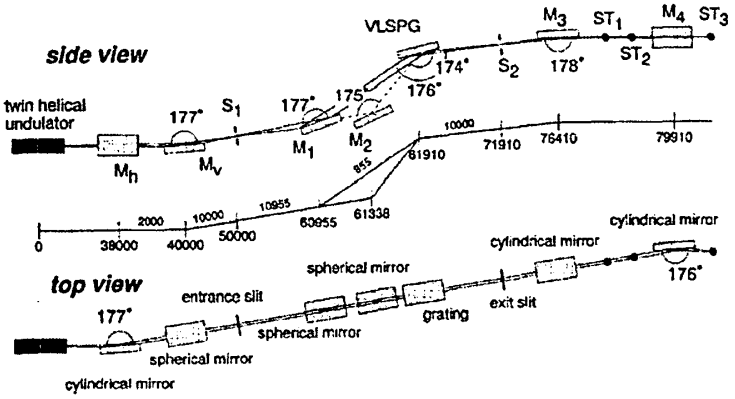

SPring-8 の BL25SU 軟 X 線ビームラインの光学系非等間隔平面回折格子を用いて世界最高分解能を実現している．Y.Saitoh et al., Rev.Sci.Instrum.71,3254(2000)

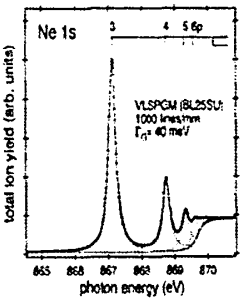

光学系の性能：860eV で 20,000 を越えるエネルギー分解能が実現している

Above 1500 eV, Bragg diffraction by single crystals is used for getting monochromatic X-rays. If the white X-ray is incident on the surface of a single crystal with the inter plane distance d, the diffraction takes place for the condition of

$$2d\sin\theta=m\lambda,$$

where θ is defined as a supplementary angle of α defined in the case of diffraction grating. Here m is a positive integer. The wave length resolution for the angular resolution is given by $\Delta\lambda/\lambda=\cot\theta\cdot\Delta\theta$. Therefore higher resolution is realized for larger θ closer to normal incidence. Two terms contribute to Δθ. One is the divergence of the X-ray from the light source and the other is the width of the rocking curve of the crystal, which depends on the individual material and its quality. The rocking curve width ranges from about 1 to 10 seconds. 10 seconds correspond to ~5×10^{-5} radian and are comparable to $1/\gamma$ at 8GeV, which is 6.2×10^{-5} radian. In order to use the high resolution X-rays a proper combination of the light source and diffraction crystals is therefore required. 2d is a characteristic material parameter and for example 6.271A for Si(111) surface. The crystal plane is defined by the Miller indices (hkl) and the inter plane distance d for a cubic crystal with the lattice constant a is given by $d=a/(h^2+k^2+l^2)^{1/2}$. Therefore higher order indices plane such as (220), (311) or (533) can be used to realize smaller Δθ and higher energy resolution. In fact, high energy resolution is often realized

by double crystal monochromators. Channel cut crystal is also used for this purpose. According to the Bragg diffraction equation, the higher order light with λ/m is also diffracted to the same direction as the fundamental radiation with λ. By setting the two crystals with a small angle offset from the parallel configuration, however, one can drastically reduce the intensity of the higher order light by two successive diffractions.

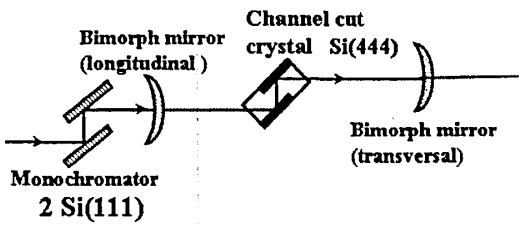

8keV 付近で 50meV 程度の分解能を実現する X 線光学系の模式図
試料上の集光は左右上下とも 100μm 以下に出来る

In order to focus the monochromatic radiation, reflection mirrors with such surfaces as spherical, toroidal, parabolic shapes are employed for wide energy region in addition to bent crystals for X-rays. As one example, the focusing by toroidal mirror is discussed. Let us assume the horizontal and vertical curvatures (radii) of the toroidal mirror as ρ_h and ρ_v and the distance from the light source to the center of the mirror as s, where the incidence angle from the mirror surface normal is α. Then the distances of the horizontal and vertical focusing s_h and s_v are given by

$1/s+1/s_h=2/\rho_h \cdot \cos\alpha$ and

$1/s+1/s_v=2\cos\alpha/\rho_v$.

The focused image by toroidal mirrors has astigmatism and a point focus is usually very difficult.

3) Electron energy analyzer

The retarding type analyzers were used in the early stage of PES. These can collect wide angle of photoelectrons but the energy spectra are only derived by differentiating the measured signals. Deflection type analyzers such as parallel plate analyzer, cylindrical mirror analyzer (CMA) and hemispherical analyzer were then developed. The hemispherical analyzer is now most often used for high resolution measurement. Historically, the hemispherical deflector analyzer was used for energy analysis of charged particles and then applied to UPS (ultraviolet PES). CMA is superior to hemispherical analyzer with respect to the acceptance angle and luminosity (the product of solid angle and sample area) by one order of magnitude for the same relative resolution when the single channel detection is employed. On the other hand the hemispherical analyzer has an image plane, where different energies can be detected

simultaneously and the distribution in one additional dimension (emission angle or position) can be detected. These advantages compensate the lower luminosity than CMA. An input lens is often attached to the hemispherical analyzer providing more space around the sample and the scanning of the spectrum can be easily realized with the constant pass energy (or constant resolution). One important requirement for hemispherical analyzer to realize high performance is how to terminate the spherical field at the entrance and exit slit. Although elaborate terminating electrodes have been used, it is possible to terminate the field with a simple plane electrode when the entrance direction is correctly set.

静電半球アナライザー

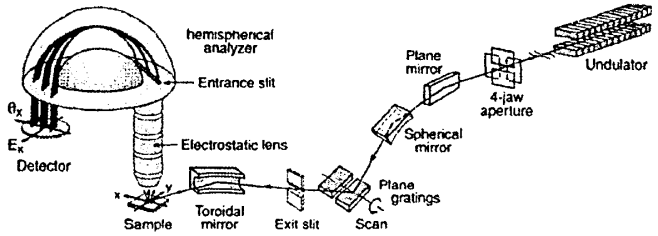

光電子分光系の１例
ALS のホームページより

If the illuminated sample is located in one of the analyzer focal planes, the detector should be located in the other focal plane. Then the spectrum is measured by changing the inter-electrode voltage. However, this method has such a drawback as the varying resolution over the spectrum. The use of multidetector is also very difficult. It is therefore desirable to keep the analyzer pass energy constant and sweep the voltage between the sample and the analyzer to get the energy spectrum with a constant energy resolution. Depending upon the kinetic energies of photoelectrons (or hν), either acceleration or deceleration of photoelectrons is required for a certain pass energy of the analyzer. An electron lens is mounted between the sample and the entrance of the analyzer to satisfy this requirement with minimum variation in transmission efficiency. A series of coaxial and rotationally symmetric electrodes are used in a lens, whose first element is in the same potential as the sample and the last element is in the same potential as the analyzer central potential. The sample is imaged onto the analyzer's entrance plane. A computer control of the lens elements voltages is required for measuring the energy spectrum. The emission angle dependence can be measured also as a dependence on the displacement over the entrance slit by a different voltage set. In this case simultaneous detection of the energy spectrum and angular distribution is feasible by use of two dimensional (2D) detector.

If the inner and outer radii of the hemispherical analyzer are R_1 and R_2 with the radius $\rho=(R_1+ R_2)/2$ of the central electron orbit, the kinetic energy of the electron

passing through the central orbit is given by $E_K = eVp/(R_2/R_1 - R_1/R_2)$, where Vp is the voltage difference between the inner and outer spheres. Thus the E_K of the photoelectron is evaluated by considering the geometrical factor and the retardation potential.

Electron counting is a popular technique for PES. Although a channeltron was used for single channel detection, MCP (micro channel plate) combined with a proper readout is used for multichannel detection. Nonlinearities in the analyzer energy scale and the image distortion can be handled by the computer. Either TV camera detection of a phosphorescence screen behind the MCP or resistive anode behind MCP is employed for 2D detection. For high resolution PES measurement by means of deflection analyzers are required good magnetic shielding below 10^{-7}T (100nT, where a 1eV electron has a radius of motion of 34m) and extremely stabilized electrode voltages in meV range. The homogeneity of the work function over the electrode surfaces is also quite important.

The simplest analyzer may be the plane mirror analyzer (PMA) made of two parallel plates 1 and 2 separated by the distance d. the plate 1 has two slits separated by L. The entrance and exit angle from this plate 1 is defined as α. Their potentials are set to V_2 and V_1. The electrons passed through the entrance slit follow the parabolic trajectory and pass through the exit slit when $V_1 - V_2 = 2E_Kd/eL$, where E_K is the electron kinetic energy. The plane mirror analyzer is very simple but has the disadvantage of low transmission, which is overcome by the cylindrical mirror analyzer (CMA) with the acceptance azimuthal angle up to 2π radian. CMA was probably the most widely used analyzer in the past for surface science. The deflection field is formed by two concentric cylinders with radii R_1 and R_2 ($R_1<R_2$), where the potential applied are V_1 and V_2. The electrons generated at the source point S pass through a 2π radian entrance slit with an opening width of w in a cylinder with a radius of R_1-h_1. The field free region is defined between R_1-h_1 and R_1. The electrons enter the analyzing field with an angle α defined in the next figure. The electrons are deflected by the field between two cylinders and then pass the field free region between R_1 and R_1-h_2. The full 2π azimuthal angle is available for detection. Among variety of selections of geometrical parameters for practical apparatuses, $(h_1+h_2)/R_1=2$ and $\alpha=42.3°$ are widely accepted to achieve the second order focusing. In this case $E=1.3e(V_1-V_2)/ln(R_2/R_1)$ and $L=6.1R_1$. The CMA is suitable to high sensitivity at moderate resolution. In some experiments double stage CMAs are applied.

In accord with the progress of angle resolved photoelectron spectroscopy, two dimensional detectors are developed to simultaneously detect the photoelectrons emitted to different directions and save the total measuring time. Since the

conventional photoelectron spectroscopy is a surface sensitive method, the reduction of the measuring time can somehow overcome the surface contamination with time. The first practical 2D analyzer was equipped with ellipsoidal mirror with the sample at one focusing point and the entrance of the analyzer at the other focusing point of the ellipsoid. Since the angle onto the detector is not equal to the emission angle, the image on the screen is inevitably distorted and numerical transformation to restore the original angular distribution pattern. Wide collection angle is also difficult to realize in this design and manufacturing of accurate ellipsoidal surface is also a hard job.

Later a 2D display type analyzer with a simpler design is developed as shown in the next figure. The synchrotron radiation introduced from a small aperture through the electrodes (functioning as obstacle-rings) hit the sample and excite photoelectrons which pass through the small concentric hemispherical grids and then enter the space

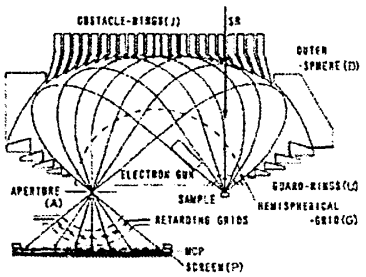

2D 光電子分析器。広い角度を取り込める。
また光電子の放出角度分布が歪まない。
H.Nishimoto, H.Daimon, S.Suga 他,
Rev.Sci.Instrum.**64**, 2857(1993)

surrounded by a larger hemispherical grid (G). The guard rings (U), partial hemispherical electrode and obstacle rings (J) provide spherical Coulomb field inside the analyzer and function as a low pass filter. Aperture A has a diameter of 1mm and located at a mirror symmetry position of the light focus on the sample with respect to the center of the grid G. The distance between the sample and aperture A is 100mm in this case. After the aperture A are located retardation grids functioning as a high pass filter. The detector part is composed of the microchannel plate and a phosphorescence screen. The shape of the inner surface of each obstacle ring is a part of the sphere with specific angle and radius. The potential on each obstacle ring is set to a proper value to realize the spherical electric field. The acceptance cone can be as large as ±50°. The advantage of this analyzer is the emission angle is exactly the same as the detection angle, which means the angular patterns are measured without distortion and the results recorded on the screen do not require any distortion correction by computers. A typical results for Kish graphite is reproduced in the next figure [1], where the change of the two dimensional angular distribution of photoelectrons from different binding energies E_B are clearly resolved for the incident light with a horizontal polarization. The nonequivalent intensities around the six K points are well explained by the dipole

selection rule. The energy resolution can be set to 1% of the pass energy. Since the full azimuthal angle of 360° is covered by this analyzer, any artificially symmetrization is not necessary for further data analyses. The abundant information obtained by this analyzer is convenient for the application to photoelectron holography, too.

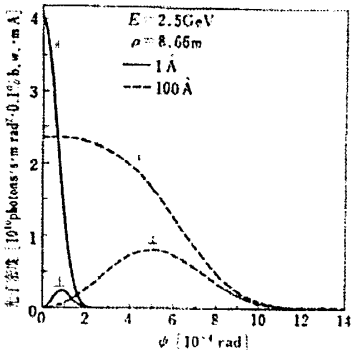

偏向電磁石部からの放射光の偏光性
水平面内では水平直線偏光　上下では若干垂直偏光成分が混ざり、楕円偏光となっている

Photoelectron spectra can also be measured by time of flight (TOF) analysis. When the photoelectrons are excited by a pulsed light and emitted from the sample, the dispersion of the velocities (energies) is induced in a field-free drift region. Although the duty cycle is rather low, the whole range of velocities can be detected as a function of time. TOF analyzer matches well with pulsed synchrotron radiation with accurate repetition. Relatively large opening angle is easily realized in this detection because no deflection field is required.

Its time resolution is limited by the 1) pulse width of the excitation light, 2) drift length, 3) size of the light focus on the sample in addition to the intrinsic time resolution of the detector. The pulse width of synchrotron radiation ranges from ns down to 0.1ns. In the case of free electron laser, it is tens fs and the shortest pulse of laser can be a few fs. The final energy resolution $\Delta E/E$ can be estimated as

$$\Delta E/E=[(2\Delta t/t)^2+(2\Delta l/l)^2]^{1/2},$$

where Δt stands for the total time resolution and Δl represents the uncertainty of the flight path to the detector. Δt is determined by timing capabilities of the electron multiplier detector and associated electronics, together with the synchrotron light pulse width. The contribution of the detector and electronics can be <70 ps, whereas the light pulse width may be sometimes larger. If Δt is ~300ps, the first term gives the

contribution of 40meV at 10eV for a typical drift tube length of ~30cm,.

Δl results from finite source size as well as the finite collection angle. The angular acceptance of ±3° provides the energy uncertainty of 0.25%. However, a much larger contribution comes from the finite source size. For 1mm source size the contribution is about 0.7%. TOF PES has been so far mostly applied to gas phase samples to utilize its high count rate. An interesting device is the double TOF spectrometer, which can be used for coincidence detection of photoelectrons and photoions.

4.Samples preparation and characterization

Clean surfaces are usually required for PES. If the surface is not clean from the beginning or gradually damaged with time, it is very difficult to obtain reliable results. Therefore the UHV condition is a necessity condition for PES. For low temperature measurements this requirement is very stringent because of the noticeable adsorption of gases onto the clean surfaces, which distorts the valence band and core level spectra. In PES below 1keV, the UHV better than low 10^{-10} Torr is usually required.

In the case of single element metals and alloy metals, ion sputtering by Ar, Kr or Xe followed by annealing are often employed to obtain clean crystalline surfaces. The samples can be mounted on Mo, Ta, and other metallic substrates via wires or nails such as Ta and W. The materials except for the samples should have low outgassing at the elevated temperatures. In the case of compounds, however, great care should be paid whether the chemical composition is the same as the starting material and the surface quality after these treatments should be checked by low energy electron diffraction (LEED) and Auger electron spectroscopy (AES).

Scraping by use of a file was often employed to get clean surfaces of fragile compounds for XPS, because the scraping could be repeated many times under the similar condition. However, the damage of the surface is unexpectedly serious in many cases and the electronic structures in the region accessible by PES are often noticeably modified from those in the undamaged clean surface. As far as the sample size is big enough and allows either fracturing or cleaving, the latter treatment is recommended except for some special cases.

Fracturing and cleaving are performed by use of either the knife edge cutting or pin post tearing schematically shown below:

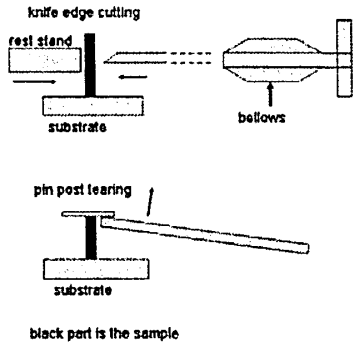

ナイフ刃による破断やへきかい、ならびにピンポスト利用の破断やへきかい。へきかいとなるか破断となるかは試料に依存する。低温下の試料に対してもこのような操作が可能

In some cases grooves are engraved in advance in the atmosphere onto the surface to facilitate the fracturing. The sample should be mounted on a metal substrate. The knife edge made of a very hard steel mounted on a linear feedthrough is pushed onto the sample surface with enough power to fracture even very hard samples. The knife edge part connected to a rod is vacuum sealed by welded bellows. In order to support the sample against the applied power, a rest stand should be touched to the opposite side of the sample. If the whole vacuum chamber has two free ports (typically 70mm$^{\phi}$ flange) located at 180°, the linear feedthrough for knife edge is mounted on one flange and the rest stand is mounted on the other flange. Both should be retracted when they are out of use. Even if there were only one available port, a special instrument with a rest stand and a movable knife edge can be used for this purpose by use of two welded bellows. Depending upon the individual sample, cleavage is sometimes realized by this instrument. Cleavage is, however, better realized by the pin post tearing in most cases of 2 dimensional crystals and in some crystals with easy cleavage planes. One wobble stick is enough for this purpose. Even in these cases, fracturing takes places sometimes instead of cleavage. Some attention should be paid in these cases to check whether the grain boundaries are not exposed to the detection. It is empirically known that the angle resolved PES measurement (ARPES) to probe the momentum dependence is only successful in the case of specular surfaces. ARPES is not applicable to fractured surfaces. In these cases, the samples are mostly glued to the substrate by means of conductive epoxy and organic insulating epoxies. The contact surfaces of both the sample substrate and the sample should be roughened in advance by scraping to provide enough surface area for bonding. The conductivity after the fracturing is the necessity to perform PES without charging up. Therefore the conductive epoxy is often put in the central part, which is then surrounded by the organic epoxy before putting the sample. Colloidal graphite is painted surrounding the insulating epoxies to be free from the possible charge up effect. Then the substrate with the sample is heated up to 150°C for 5–10 minutes to harden the epoxies. It is possible to do the PES measurement

in low 10^{-10} Torr. In order to do very low temperature measurements, better thermal contact is required. To realize very low sample temperature and protect surface adsorption, the sample mounted on a He flow cryostat is further thermally shielded (surrounded) by cold shield (s) of additional He cryostat(s). Such a condition is necessary to realized 1 meV resolution, because the broadening by the Fermi-Dirac distribution function is around $4k_BT$ (1K corresponds to the broadening of ~0.3 meV)

Usually a few samples glued to sample substrates are stored in a sample bank in the entry air lock system, whose vacuum is typically 10^{-7} Torr evacuated by a turbo–molecular pump. One particular sample is selected and transferred to the sample preparation chamber, where such treatment as ion–sputtering, fracturing or cleavage can be performed under the proper condition. In some cases, however, the fracturing or cleavage at low temperatures is really required to reduce the thermal diffusion of impurity atoms toward the surfaces. In such a case the treatment should be done in situ on the sample mounted at the top of the variable temperature cryostat.

On the other hand high temperature measurement at several hundred °K requires careful outgassing of the local surrounding before cleaning the sample. In such a case the glue is not usually applicable because of the high outgassing rate. The sample should be mechanically supported by wires or clamps. The sample should be locally heated up in order not to induce the outgassing from the local environment.

As for the samples, it is also possible to grow crystals in a sample preparation chamber connected to the analyzer chamber. In addition to classical methods of evaporation by heating the starting materials, electron beam induced sputtering is used for evaporating such as materials as Fe, Co and similar materials. In the case of compounds and alloys, molecular beam epitaxy (MBE) or pulsed laser deposition (PLD) can be utilized. Since SR and laser light beam can be focused into a small spot nowadays, measurements of the composition dependence or the thickness dependence of the electronic structures are feasible, if the sample composition and thickness are varied laterally in the sample with large enough sample size.

Surface structural analysis can be performed not only by LEED but also by RHEED. In the case of surface sensitive PES, the presence of the surface super lattice and surface relaxation strongly modifies the electronic structures. Therefore surface characterization is a prerequisite to discuss the obtained experimental PES results.

5. Fundamental concepts and methodology

It is quite important to understand the inelastic scattering processes of photoelectrons in solids. The electron with energy E_f created at depth z below the

sample surface has some probability to reach the surface without inelastic scattering. Inelastic scattering with phonons may cause the energy loss of the order of several tens meV and becomes important in low kinetic energies as shown in the next figure. More serious inelastic scattering is due to the electron-electron scattering. In this process the part of the original energy E_f is transferred to other electrons. The secondary electron background increasing with the increase of the binding energy results from inelastic scattering processes. The values of inelastic mean free path (hereafter abbreviated as mean free path: λ_{mp}) can be experimentally evaluated by transmission of photoelectrons through overlayers. The nomenclature of attenuation length is employed in this case. Both quantities are not necessarily the same, since the elastic scattering in the overlayer may contribute. After accumulation of many results, the so-called universal curve is obtained as schematically shown in the next figure.

平均自由行程の評価の３つの例

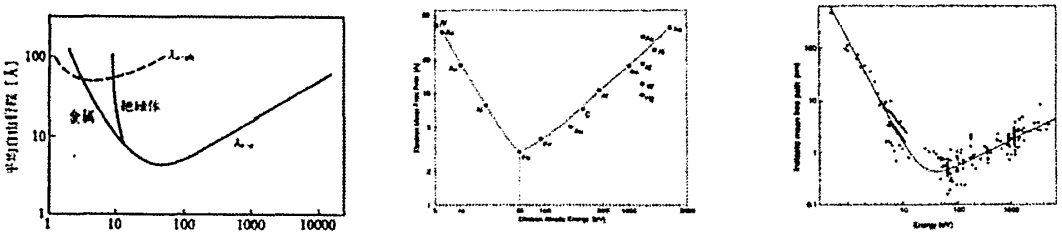

The mean free path due to electron-electron scattering is known to be material dependent but generally has a minimum in the energy region of 20~100eV. The minimum value is less than 10A and sometimes close to 3~5A. This means that the observed photoelectrons carry the information over only few layers of the sample surface. Namely the information on the bulk as well as the surface is included in the observed PES spectra and the separation into surface and bulk components is not a straight forward job. In order to realize bulk sensitivity with high resolution, soft X-ray PES in the region of E_K~500–1000 eV has been developed. Still bulk spectral weight remains in the range of 60–70%. Then higher bulk sensitivity is expected for E_K~3–10 keV by use of hard X-ray excitation. Then bulk spectral weight reaches more than 95% for E_K above 8keV, where λ_{mp} becomes close to 100 A. The high bulk sensitivity is also reported for several materials below E_K~5 eV. In the case of insulators, it is known that the mean free path increases with decreasing energy below the band gap energy of the material. The short mean free path inevitably requires clean surfaces for the study of PES. The surface science is therefore strongly promoted by utilizing this

characteristicStill UHV in 10^{-10} Torr region is usually required for conventional PES measurements to keep the surface condition during the measurement time.

If the angle of the electron motion to the surface is θ from the sample surface normal, the probability of the photoelectron created at z~z+dz from the sample surface to reach the surface is estimated by

$$\propto \exp(-z/\lambda_{mp}\cdot \cos\theta)dz.$$

For the normal emission with θ=0° the probability of the electron to escape from the surface without inelastic scattering is 1/e for $z=\lambda_{mp}$. With increasing z, the probability decreases monotonously. If there were a surface layer with thickness of s, in which the electronic structures are different from those in the bulk, the measurement of photoelectrons with the mean free path λ_{mp} provides the bulk spectral weight of $\exp(-s/\lambda_{mp})$ and the surface spectral weight of $(1-\exp(-s/\lambda_{mp}))$. In the case of angle integrated PES, the deconvolution of the surface and bulk components is possible under some assumptions. However, very little is known about inelastic scattering effect in angle resolved photoelectron spectroscopy for valence bands. In this case, comparison of high and low energy ARPES is quite important to see the effect of the surface and to derive the information on bulk band dispersions.

Photoionization cross section σ is another important concept to be kept in mind for PES. As shown in the next figure, σ depends strongly on hν. For example, O2p state has high σ at low hν while it decreases with hν remarkably. At high hν above several hundred eV, transition metal (TM) 2p and rare earth 4f states have relatively much higher σ than TM 3d and O 2p states.

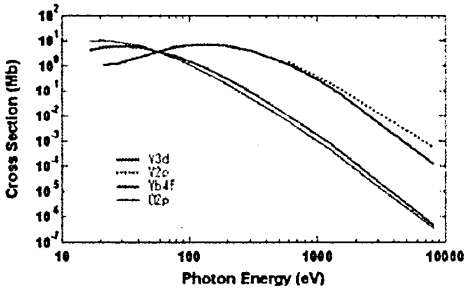

10keV
上から
V2p
Yb4f
V3d
O 2p

光イオン化断面積の
hν依存性の例

Therefore proper choice of hν considering these factors is quite important. Concrete examples are lectured later.

For theoretical analyses, sudden approximation is employed. This means that the response of the system to the creation of the photohole is assumed to be instantaneous and that there is no interaction between the escaping photoelectron and the remaining system. This approximation is valid for high energy limit. However, the validity of the sudden approximation is not guaranteed in low hν PES. Matrix element effect is

another critical factor in ARPES in low hν region, providing very complex hν dependence of the photoemission intensity.

In the photoelectron excitation process, an electron in the occupied state is excited by photons to the unoccupied state and escapes into the vacuum. Although occupied valence band states can be probed at low hν, deep core level states can be only probed by high hν. Let us define the energies of the Fermi level, the vacuum level and the photoelectron kinetic energy in the vacuum by E_F, E_V and E_K. E_F is located in the band gap in the case of the semiconductors and insulators and the exact location depends upon doping in the case of semiconductors. In the case of metals, E_F is in the conduction

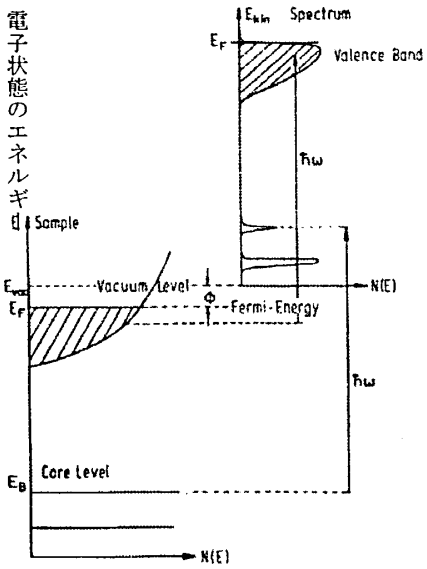

光電子励起の模式図
真空準位とフェルミ準位のエネルギー差を仕事関数と呼ぶ

band. The photoelectron can escape into the vacuum when its energy is above $E_V - E_F$, which is called the work function ϕ and E_K is scaled from E_V. In the system with negligible electron correlation, the binding energy E_B of the electron responsible for the photoelectron is evaluated as

$$E_B = h\nu - E_K - \phi$$

according to the Koopman's theorem. Since E_K is measured by an electron energy analyzer and ϕ is evaluated from the secondary electron cut–off by the vacuum level, the E_B is evaluated by the photoemission experiment. The photoemission intensity plotted as a function of E_B is called energy distribution curves (often abbreviated as EDC). The photoelectrons following these equations can be called primary electrons, whereas part of the energy of photoelectrons is transferred to the surrounding electrons by electron–electron scattering on the way of the motion. There are also Auger decay process where the shallow occupied electron decays into the core hole and other occupied electron is excited with receiving the same amount of energy. Such electrons emitted into the

vacuum are called Auger electrons. These electrons are also subjected to the electron –electron scattering. The electrons thus produced are called secondary electrons, which are accumulated as E_B increases (or E_K decreases).

When hν is varied, one recognizes sometimes a dramatic enhancement of the photoemission intensity of some particular orbit in some particular binding energy region. This phenomenon is known as a resonance photoemission, which is very prominent in the case of rather localized state such as d or f states. This technique is quite powerful to extract the electronic structures related to low concentration atoms and the states with low photoionization cross section under the off resonance condition. The Ce 4f state is one of such examples. In this case how to extract the electronic states related to the 4f states is a very important subject from the standpoint of view of Kondo physics and valence fluctuation.

The resonance enhancement of the 4f state is expected for the resonance excitation of either the 3d core or 4d core state. For simplicity, the 3d–4f resonance photoemission is explained below. The direct photoemission of the 4f state is generally described as

$$3d^{10}4f^{1} \rightarrow 3d^{10}4f^{0}\varepsilon l, \quad (1)$$

where the 3d state is included for completeness and εl stands for the photelectron. In parallel to this process, the strong 3d→4f core absorption takes place when hν is tuned to this threshold. This process is described as

$$3d^{10}4f^{1} \rightarrow 3d^{9}4f^{2}. \quad (2)$$

The core hole relaxes either via radiative recombination or nonradiative process. If the 4f electron relaxes down nonradiatively to the 3d core level, the energy can be transferred to the other 4f electron, which is excited far above the Fermi level. This process is called as a direct recombination process and can be described as

$$3d^{9}4f^{2} \rightarrow 3d^{10}4f^{0}\varepsilon l. \quad (3)$$

The direct recombination is a special case of Auger decay process. If one compares the process (1) with the process (2)+(3), it is recognized that both the initial state and the final state are the same between two different processes. Then an interference is expected to take place between these two processes, resulting in resonance enhancement of the f photoemission intensity when the excitation induces an constructive interference. Often the enhancement is observed for the excitation slightly above the threshold and suppression or resonance minimum is observed for excitation slightly below the threshold. Often the difference spectrum between the resonance maximum and minimum spectrum, both properly normalized by the photon flux, is used to reveal the resonating component. When the two hν are very different, however, this technique is not reliable. The resonating behavior is not included in such a table as

J.J.Yeh and I.Lindau, Atomic data and nuclear data tables 32, 1-155 (1985).

Constant final state (CFS) spectroscopy for a fixed E_K, detecting the photoemission intensity while scanning hν was employed for sometime to detect the intermediate state. Total electron yield spectroscopy (TEY) is a method to collect all outgoing electrons as a function of hν. Most electrons are secondary electrons excited by the Auger decay process. The number of electrons excited by this process is proportional to the number of core holes. Therefore the total electron yield spectrum is empirically very similar to the core absorption spectrum. Since the absorption coefficient is very high in the soft X-ray region, the absorption measurement requires very thin free-standing film to perform the transmission-based absorption measurement. Thus the total electron yield is very conventionally employed to measure the soft and hard X-ray absorption of splids.

6.Angle integrated photoelectron spectroscopy

Very many results of valence band spectra of semiconductors and metals by angle integrated photoelectron spectroscopy have been so far reported in literature. Although the band dispersions are studied only by the angle resolved measurements on specular single crystal surfaces, gross features of the valence bands and DOS can be studied by angle integrated measurements on non-specular surfaces of single and polycrystalline solids. Some results of semiconductors and transition metal oxides, which have either weak or noticeable electron correlation are reviewed here.

The electron correlation or repulsive Coulomb interaction is quite weak in conventional semiconductors as Si, Ge, GaAs and so on, where the Koopmans' theorem can be safely applied and the DOS can be relatively easily estimated from PES. The results of conventional semiconductors are referred to in literature (L.Ley and M.Cardona, Photoemission in Solids, I, II, Topics in Applied Physics, Springer). Here is shown an example of layer semiconductor black P. The ultraviolet PES and XPS are shown in the top and middle panels in comparison with the result of self-consistent pseudopotential band calculation at the bottom.

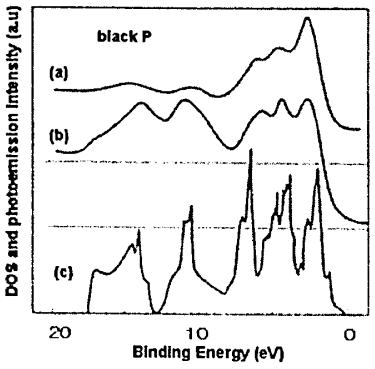

層状半導体黒リンのPES(110eV、1253.6eV）とバンド計算による状態密度

The weak shoulder at ~1.2eV and three structures at ~2.7, ~4.7 and ~6.6eV can be mainly assigned to the P 3p orbitals, while the peaks at ~10.8 and ~15.4eV are assigned to the P 3s orbitals. The relative increase of the intensity of the 4.7eV peak with increasing hν above 40eV may suggest significant admixture of the P 3s component as suggested by the tight binding band calculation. A Fano type resonance interference of the 2.7eV peak is clearly observed for the P 2p core exciton excitation (not shown). However, the magnitude of interference is smaller than the case of strongly correlated electron systems, reflecting the extended character of the P 3p states.

The metal to insulator transition (MIT) and accompanying change of the electronic structures is one of the central issues of the present solid state physics. There are many reports of PES on MIT in the cases of V, Mn, and other compounds. VO_2 is a d^1 system which shows clear first order MIT near T_t=340K. In the metallic (M) phase above T_t, it has a TiO_2 type rutile structure whereas it has a monoclinic structure in the insulator (I) phase below T_t. The PES measured with modest resolution on cleaved surface are shown in the next figure with the dashed and solid curves for the M and I phases at 375 and 298K. The dotted curves represent the spectra deconvoluted with the instrumental resolution of 0.25eV. In the M phase are seen two structures in 0–2eV, which are now definitely ascribed to the coherent peak and incoherent part by bulk sensitive high resolution PES. In the I phase is seen a peak at ~0.78eV and the band gap opening. The experimental results are consistently interpreted as due to the interplay of strong

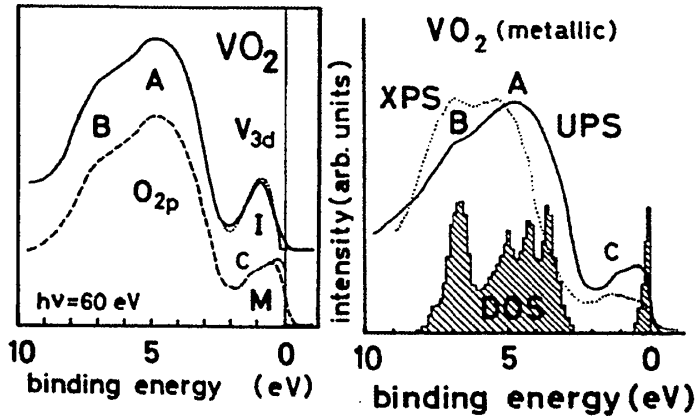

Phys.Rev.B 41,4993(1990).

Coulomb interactions and structural distortions playing a crucial role for the MIT.

Changes of electronic structures accompanying other phase transitions are also interesting subjects of PES. One example of 1T–TaS_2 is shown here [2]. This material shows MIT together with the charge density wave (CDW) phase transition. The above right figure shows the angle integrated PES of the $1T_1$ incommensulate, $1T_2$

quasi-commensulate and $1T_3$ commensulate CDW phases. The right panel shows the valence band measured at hν=21eV and the left panel shows the Ta 4f core spectra measured at hν=66eV for comparison purpose. The valence band spectra clearly show the MIT from the $1T_2$ to the $1T_3$ phase. Further details of the valence bands are studied by angle resolved measurement. From the Ta 4f core level splitting, one can discuss the inequivalent potentials at different Ta sites and check the validity of the proposed model.

Fe_2O_3 is an antiferromagnetic insulator and crystallizes in the α-corundum structure with an Fe atom octahedrally coordinated by six O atoms. This material called hematite belong to the charge-transfer insulator like NiO rather than the so-called Mott insulator. Next figure summarizes the PES measured for a wide range of hν with modest resolution. Broad spectral shapes are observed with some features at ~2.5, ~5 and ~7 eV. According to the ligand field theory the former two structures are assigned to the d^4 final state multiplet (^5E_g and $^5T_{2g}$) from the high spin d^5 ground state and the third one to the O 2p band. However, this simple interpretation is not fully acceptable

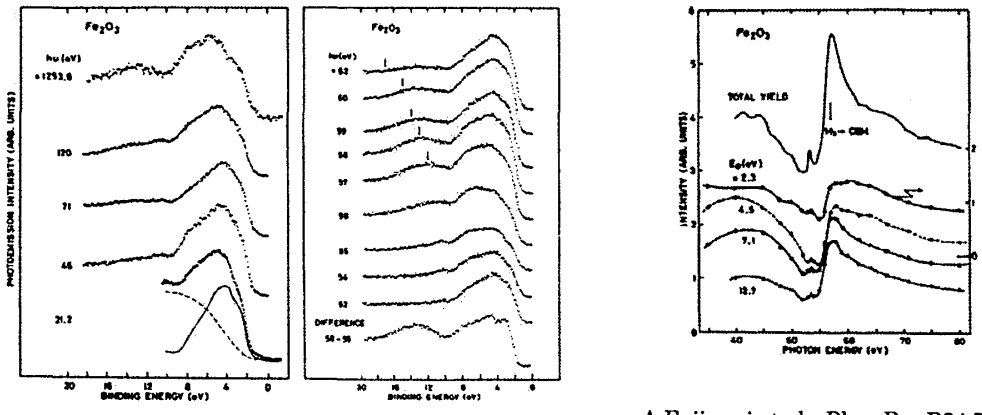

A.Fujimori et al., Phys.Rev.B34,7318(1986)[1]

from the following reason. The photoionization cross section of the O 2p states relative to that of the Fe 3d states is known to increase toward lower hν in the present hν region. The Fe 3d states are expected to be much weakened below hν=40eV. However, the observed spectral shape does not change much with decreasing hν, suggesting strong hybridization between the Fe 3d and O 2p states. The spectrum at hν=21.2 eV is mostly ascribed to the O 2p peak, where the higher energy part at ~8eV is somehow suppressed. The structure at ~4eV is ascribed to the O 2p nonbonding state and the Fe 4sp-O2p bonding states are located around ~8eV.

A general experimental approach is the resonance PES with changing hν. 3p-3d resonance is employed as shown in the middle panel. For the excitation above the Fe 3p core threshold, the $M_{2,3}M_{4,5}M_{4,5}$ Auger emission appears at a constant kinetic energy

whose expected energy is shown by the vertical bars. This Auger feature is not overlapping with the valence band structures in the region of 2–8eV. The resonance behavior of the valence band structures is clearly seen as shown by the CIS spectra in the right panel. Even the structure near 7eV shows the resonance behavior with a minimum and a maximum below and above the threshold, suggesting the noticeable contribution of the Fe 3d component. The Fe 3d component can be empirically extracted by taking a difference spectrum between the two spectra measured at the resonance maximum and minimum as shown at the bottom.

In order to interpret the Fe 3d spectrum, the configuration interaction cluster calculation can be applied as shown in the next figure. The ground state is assumed to be a linear combination of the $|d^5\rangle$ and $|d^6L\rangle$ states and the final states are represented by the mixing between d^4, d^5L and d^6L^2 configurations, where L stands for the ligand hole. The correlation energy U is explicitly taken into account in the calculation. The decomposition of the whole spectrum into the three different configurations is given in the bottom. The experimental results are well explained.

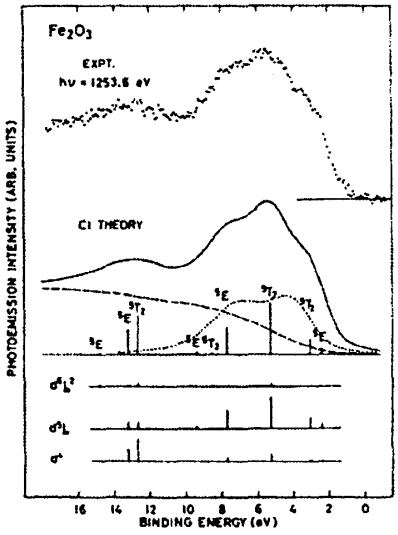

A.Fujimori et al., Phys.Rev.B34,7318(1986)

Core level spectroscopy has been widely applied for chemical analyses. One of the example is the surface core level shift as shown in the above right figure for GaAs on the (110) cleaved surface [3]. When the proper hν with the highest surface sensitivity is employed for the measurement, additional structures are observed in additional to the conventional spin-orbit split As 3d and Ga 3d core level doublet. Among the two corresponding spectra, the upper spectra have higher surface sensitivity, where noticeable bump is observed on the lower (higher) energy side for As (Ga) 3d core level. According to a proper deconvolution, the surface spectra (S) are separated from the bulk

spectra (B) as shown by the dashed curves. The S components are found to be decreased for smaller kinetic energies as ~10eV compared with the results for the kinetic energies of ~40eV in agreement with the increase of λ_{mp}, which is estimated as 19 A at ~9eV compared with 5.9 A at ~40eV. The opposite shifts of the core levels on the surface are interpreted as due to the initial-state charge transfer accompanying with the surface relaxation, where the surface As atoms move outwards and surface Ga atoms move inwards with a ~25° bond-angle rotation and a charge transfer from Ga to As. The bulk Ta 4f core level splitting in $1T_3$ phase of 1T-TaS_2 can be likewise interpreted as due to the inequivalent charge densities at different Ta sites.

The presence of satellite structures is widely known in the case of core PES of transition metal compounds. One of the examples is shown for Fe_2O_3, where the PES of Fe 3p, Fe 3s and Fe 2p cores excited by Mg Kα source are shown in addition to the valence band XPS. The Fe 3p, $2p_{3/2}$ and $2p_{1/2}$ core levels are accompanied with a satellite structure on the higher energy side. Meanwhile, two satellite structures, one prominent and the other rather weak, are observed in the case of the Fe 3s core level. The splitting of the satellite from the main peak is different in the case of Fe 3s core compared with those of Fe 3p and 2p core levels. In contrast to these Fe core levels, no satellite structure is observed for the O core levels. The origin of the satellites is not due to such an energy loss process as plasmons but due to the excitation or screening involving the Fe 3d orbitals at the core-hole site. According to the similarity of the satellites between

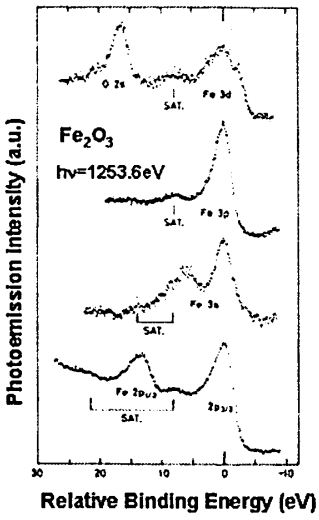

A.Fujimori et al., Phys.Rev.B34,7318(1986)

the core level and valence band, the main line of the core PES is interpreted as well screened $c3d^6L$ final states where the core hole c is screened by the charge transfer from the ligand to the 3d state, whereas the satellites are the poorly screened cd^5 final states.

This interpretation is in contrast to the traditional one which assumes a shake-up transition from the ligand to the 3d state.

The Fe 3s core level in Fe_2O_3 is not simply split into the ^7S and ^5S components by the spin exchange interaction with the magnetic $3d^5$ shell but shows rather complicated structures. In fact, not only the intra-atomic exchange splitting but also the charge transfer and the final-state core-hole screening are responsible for the observed structures. Cluster model calculations taking these effects into account are now available for core levels.

Multiplet structures in PES are most clearly observed in rare earth systems with localized and open 4f shells. In many cases of rare earth compounds except for some Ce, Pr, Sm, and Yb compounds, the valence of the rare earth atom is very close to trivalence, where 4f electrons are rather localized and atomic-like. With the increase of the atomic number, the 4f wave functions decrease as known as lanthanide contraction. Their 4f PES spectra are therefore predicted by the atomic multiplet calculation as reported in many literatures. The 4f charge remains inside the mean extension of the rare earth 5s, 5p, 5d and 6s shells. When the binding energies of the 4f states is very low, however, they can participate in the formation of bonds. The 5d states form bands in solids and they determine the atomic radii which remain almost constant for most trivalent lanthanides. If the hybridization between the 4f states and the conduction band states is noticeable, the valence fluctuation (VF) can take place, where the multiplets resulting from two initial configurations (f^n and f^{n+1} or f^{n-1}) can be observed by PES. Such an example is most clearly shown for Ce, Sm, Yb systems as explained later. In the case of Ce 3d core XPS in VF materials, $3d^94f^0$ and $3d^94f^2$ components are observed in addition to the main $3d^94f^1$ states. The relative intensities and energy positions depend upon such parameters as the magnitude of hybridization, f level energy, correlation energy, Coulomb interaction between the core hole and the outer electrons, exchange interaction, and so on.

The charge transfer satellites and configuration interaction satellites are already described in the preceding sections. In the case of free molecules, the electronic states coupled with the molecular vibrations can be observed by high resolution PES. Such an example is known for CO adsorbed on Ni(100). In the case of core XPS in solids, the plasmon satellites are often observed. If the deexcitation of the photohole induces the charge density fluctuation in the conduction-electron system, the intrinsic energy loss, so-called intrinsic bulk plasmons, are excited. The photoelectrons also lose their energies on their journey toward the surface by exciting extrinsic plasmons with a rather well defined energy loss and by inelastic scattering by electron-electron and

electron-ion collisions. The featureless smooth background results from the latter processes. It is also possible to excite the surface plasmons under some conditions. Such examples are reported for the 2p and 2s core PES for Mg metal. The discrimination between the intrinsic and extrinsic plasmons is discussed in literature. Even the overtones of plasmons are often observed. Plasmon satellites are also observed for valence bands of simple metals.

7.Bulk and surface sensitivity

The difference between the bulk and surface electronic structures is clearly demonstrated by high resolution soft X-ray PES for 4f rare earth and 3d transition metal compounds. The next figure demonstrates how the bulk sensitive 4f PES revealed by means of 3d-4f resonance are different from those reported by 2000 by means of the surface sensitive 4d-4f resonance. Namely, the bulk Ce 4f spectra of low and high Kondo temperature compounds are much different from the surface 4f spectra representing the less itinerant character. Even the Kondo tail spectra in the right panel near E_F are much different from those observed by surface sensitive PES. Most of the controversies piled up in the last two decades on Kondo materials by PES are now solved by this new bulk sensitive PES technique developed by us in SPring-8 in the period of 1997–2000.

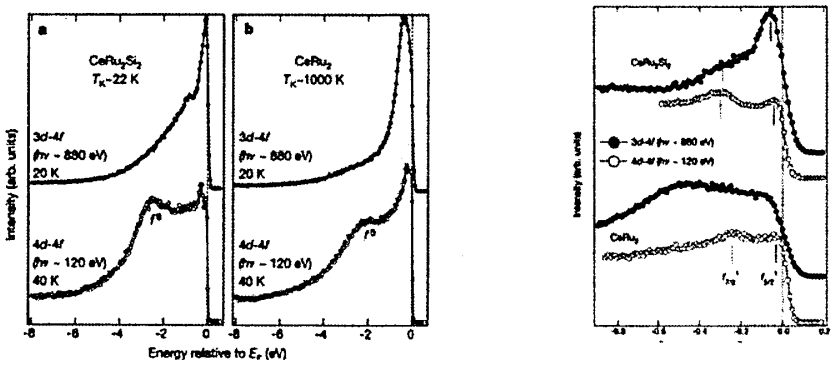

A.Sekiyama,S.Suga ほか, Nature,403,396(2000)

It is turned out that the bulk sensitivity is essential to discuss the bulk electronic structures of 4f compounds. Deviation of the PES results from the prediction of single impurity Anderson model is demonstrated recently for $YbAl_3$ by this technique.

Even in the case of 3d transition metal compounds, it is now revealed that false physics were discussed sometimes by PES performed with high surface sensitivity. One example is shown in the left panel of the next figure on $Sr_{1-x}Ca_xVO_3$, which are all metallic despite the possible correlation effect. Quite different electronic structures are reported from the low hν PES in literatures. When the cleaved or fractured samples

were measured at different hν, however, it was found that the spectral intensity of the coherent peak near E_F increased with hν in all three materials and the high hν spectra became very similar, although the 21.2 eV spectra were very different among these three materials. From these results, we can evaluate the surface and bulk spectra. It is found that the 21.2 eV spectra are quite similar to the deconvoluted surface spectra. The bulk spectra are consistent with their electronic properties probed by other bulk sensitive techniques.

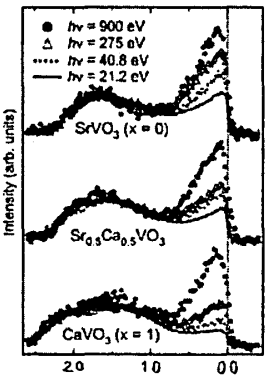

Sekiyama, Suga ほか
PRL 93,156402(2004)

Extremely low hν PES (ELEPES) became feasible by means of laser and SR light sources. The right panel shows such examples [4]. Now the total resolution down to 370 μeV is reported to be feasible. Although bulk sensitivity may be achieved, the validity of the sudden approximation and the influences of the matrix element effects in addition to the extent of the probed momentum space must be carefully examined to discuss the intensity behavior of observed structures.

Hard X-ray PES (HAXPES) is less influenced by these problems and very useful to discuss not only the valence band but also many core levels. One example is given for $YbInCu_4$, which shows bulk valence transition around 40 K. In addition to the surface layer, contribution of subsurface is so far reported by many PES. Therefore the valence evaluated even by soft X-ray PES is much smaller than the bulk value reported by other means. Therefore ~6 keV PES has been performed and the mean valence in the high and low temperature phase is evaluated as 2.9 and 2.74 from the Yb 3d core spectra. We have performed ~8 keV PES and obtained the mean valence of 2.93–2.94 and 2.76, respectively. Even in the $4f^{13}$ region near E_F fine conduction band structures and detailed behavior of the Kondo peak are resolved with much higher resolution of 120 meV. The deviation from the prediction by single impurity Anderson model is again revealed in YbInCu4. In both cases first order phase transition is confirmed. Thus the high resolution HAXPES is very important for the study of strongly correlated electron systems.

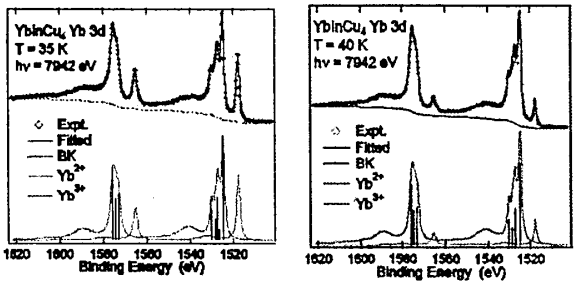

8. Angle resolved photoelectron spectroscopy (ARPES) of valence bands

The momentum of photoelectrons can be evaluated by ARPES. The mutual relation between E_B and the momentum k provides the so-called band dispersions $E_B(k)$. By tracing the crossing point of the dispersion across the Fermi energy, the Fermi surface topology can be experimentally estimated as well. Even the electron-like or the hole-like character of the Fermi surface can be judged from the whole dispersion behavior in contrast to such a method as de Haas van Alphen measurement. The methodology called Fermiology has progressed intensively through the study of high temperature Cu superconductors. ARPES has been traditionally developed for low hν excitations, where the finite value of the photon momentum q can be neglected in comparison with the electron momentum scaled by the Brilloiun wave number π/a (a is the lattice constant).

Let us assume the energy and the wave number of the electron in the vacuum as E_K and K. Likewise those for the final and initial states in the crystal are represented by E_f, k_f and E_i, k_i with using the suffix standing for the final and initial state. If the photon momentum q is negligible (which is not the case in soft X-ray ARPES as discussed later), we can assume $k_f=k_i=k$ and the energy conservation rule is applicable as

$$E_K=E_f=E_i + h\nu. \qquad (1)$$

The momentum parallel to the surface with the translational symmetry is also conserved as

$$K_{\parallel} =k_{\parallel}+g_{\parallel}, \qquad (2)$$

where the reciprocal lattice vector $g_{\parallel}$ can be neglected for simplicity.

By defining the emission angle of the photoelectron with respect to the surface normal as θ, one can evaluate the electron wave number in the crystal as

$$k_{\parallel}=K \sin\theta. \qquad (3)$$

Since $E_K=\hbar^2K^2/2m$ in the vacuum, the momentum in the crystal can be evaluated as

$$k_{\parallel}=(2mE_K/\hbar^2)^{1/2}\cdot \sin\theta. \qquad (4)$$

If E_K is represented in eV the practical equation is $k_{\parallel}(A^{-1})=0.51(E_K)^{1/2}\cdot \sin\theta$.

$E_B(k_i)$ is evaluated according to this equation. In the cases of two dimensional and one dimensional systems, the dependence on $k_{\perp}$ can be negligible and the $E_B(k_{i\parallel})$ is

experimentally evaluated. In the three dimensional systems with the noticeable $k_\perp$ dependence of the electron energy, a different approach is employed. Namely normal emission spectra are measured as a function of hν. $K_\parallel = k_\parallel = 0$ can be assumed in this case. The $k_\perp$ is, however, not equal to $K_\perp$ because the electron crosses the boundary between the crystal surface and the vacuum and the electron is strongly scattered by the surface potential. This scattering is in general strong for low energy electrons. When the conduction band dispersion $E_f(k_f)$ is known from the beginning, $k_{f\perp}$ can be evaluated from the measurement of E_K in this case. Often assumed is the following approximation

$$E_f(k_{f\perp}) = \hbar^2 k_{f\perp}^2/2m - V_o, \quad (5)$$

where the inner potential V_0 has a positive value. Then one can evaluate $k_{f\perp}$ as

$$k_{f\perp} = (2m(E_f(k_{f\perp}) + V_o))^{1/2}/\hbar = (2m(E_K + V_0))^{1/2}/\hbar. \quad (6)$$

This relation was successfully applied to many systems to evaluate the $E_B(k_\perp)$.

If the surface scattering is very weak as in the case of some layer materials, the off-normal ($\theta \neq 0$) emission can be likewise treated in the equivalent approximation. Then the following expression holds:

$$\hbar^2 k_{f\perp}^2/2m + \hbar^2 k_{f\parallel}^2/2m = E_K + V_o. \quad (7)$$

If $K_\parallel = k_\parallel$ is assumed, one can evaluate $k_\perp$ as follows:

$$k_\perp = (K^2\cos^2\theta + 2mV_0/\hbar^2)^{1/2}. \quad (8)$$

In the case of the soft X-ray ARPES, however, the photon wave number q cannot be generally neglected in comparison with the Brillouin wave number, because the photon wavelength λ is 12A, for example, in the case of hν=1000 eV and $q = 2\pi/\lambda$. If the incidence angle of the photon is θ from the surface normal, the ⊥ and ∥ component of q are expressed as

$$q_\perp = 2\pi/\lambda \cdot \cos\theta \quad \text{and} \quad q_\parallel = 2\pi/\lambda \cdot \sin\theta. \quad (9)$$

These quantities are just transferred to the photoelectron according to the momentum conservation rule. In this case $k_{f\perp} = k_{i\perp} - 2\pi/\lambda \cdot \cos\theta$, which can be evaluates as

$$k_{i\perp} = 2\pi/\lambda \cdot \cos\theta + (K^2\cos^2\theta + 2mV_0/\hbar^2)^{1/2} \quad (10)$$

By using (10) and $k_{i\parallel} = K_\parallel - 2\pi/\lambda \cdot \sin\theta$, the soft X-ray ARPES can provide the information on band dispersions in the probing depth region larger than the low energy ARPES.

The angular resolution of the electron analyzer δθ is given by the design of the input lens and the applied voltages to the lens elements together with the entrance slit width. The resolution of the wave number of the photoelectrons is proportional to $(E_K)^{1/2}$, which requires higher resolution (or smaller δθ) at higher E_K to realize the equivalent wave number resolution as at low E_K. Although δθ of ~0.1° is conventionally realized nowadays, further improved δθ will be required in ARPES for soft X-ray excitations.

An example of soft X-ray ARPES is given for Sr_2RuO_4, which is known to be a spin

"triplet" superconductor with T_C~1K. Combination of the quantum oscillation measurements and band-structure calculations suggests one hole-like Fermi surface (FS) sheet centered at (π, π) (α sheet) and two electron-like FS sheets centered at (0,0) (β and γ sheets) in Sr_2RuO_4. The FSs probed by low hν ARPES (hν< ~120 eV) on clean surfaces are strongly influenced by the surface reconstruction and could not be directly compared with the results of quantum oscillations measurements. The ARPES results on degraded surfaces obtained by cleavage at 180 K and fast cooled down were on the other hand consistent with the latter measurements. Thus the characters and shapes of the two-dimensional bulk FSs of Sr_2RuO_4 are experimentally still unclear. The high-energy ARPES was performed at hν=700 eV on (001) surface of single crystal cleaved at 20 K. The overall energy resolution was set to ~120 and ~200 meV for high-resolution measurements and FS mapping, respectively. ARPES (energy distribution curves, EDCs) along the major directions demonstrate where bands cross E_F. The momentum distribution curves (MDCs) provide k_F with better statistics when the band dispersion is steep. The integrated PES intensity from E_F to –0.1 eV above E_F is plotted in the next figure, where the hole-like (α) and the two electron-like (β and γ) FS are directly observed in consistence with the dHvA results. We find that the shapes of the α and β sheets are square-like while the shape of the γ sheet is rather circular-like. These shapes reflect that the γ sheet is mainly composed of a rather ideally two-dimensional d_{xy} band while the other square-shaped sheets are due to the d_{yz} and d_{zx} bands, which are to some extent one-dimensional in the electronic states. The combination of the observed two square-like FS sheets, the α and β sheets, can also be regarded as two one-dimensional FSs located at $k_x = \pm Q$ and $k_y = \pm Q$, where Q is estimated as ~ 0.65π from our high-energy ARPES. It has been theoretically predicted that FS nesting effect occurs with wave vectors $\boldsymbol{q} = (\pm 2\pi/3, k_y')$, $\boldsymbol{q} = (k_x', \pm 2\pi/3)$ and especially at $\boldsymbol{q} = (\pm 2\pi/3, \pm 2\pi/3)$ where k_y' and k_x' are arbitrary. An inelastic neutron scattering study indeed detected magnetic fluctuations for $\boldsymbol{q}_0 = (\pm 0.6\pi, \pm 0.6\pi)$, which could be due to the nesting properties. As shown below, the observed FSs give direct evidence for the nesting instability with $\boldsymbol{q} = (\pm 2\pi/3, \pm 2\pi/3)$.

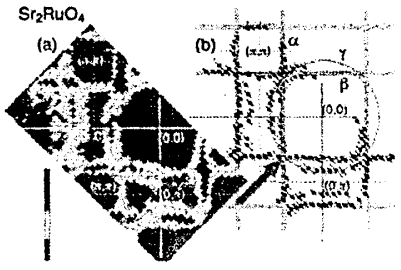

A.Sekiyama et al.,
Phys. Rev. B 70, 060506(R)1~4 (2004).

This bulk sensitive ARPES in the soft X-ray region is also applied to high Tc cuprates and new features of the band dispersion and FS are now revealed.

9. Outlook

The resolution of PES is under dramatical improvement. Resolution of 200 μeV below hν~10 eV is no more a dream. Improved cryogenic systems will be the most crucial factor toward this direction. HAXPES is also rapidly growing. The resolution of the light source itself can be better than 1 meV at the sacrifice of the photon flux. The stability of the high voltage power supply is already better than 10 m eV. HAXPES resolution may soon reaches 30 meV and further 10 meV. The low photoionization cross section may be subsidized by long measuring time, which does not much spoil the bulk sensitive HAXPES spectra. HAXARPES is a real challenge requiring higher angular resolution and serious consideration of the intrinsic k broadening effect. In spite of several difficulties, the rapid growth of PES and ARPES may not stop in the future.

References

[1] H.Nishimoto *et al.*,J.Phys:Condens.Matter 8,pp.2715-2732(1996).
[2] R.A.Pollak *et al.*,Phys.Rev.B24,7435(1981).
[3] D.E.Eastman *et al.*,Phys.Rev.Lett.45,656(1980).
[4] R.Eguchi *et al.*,Phys.Rev.Lett.96, 076402(2005).